ISSN 2321-807X

# Sol-Gel Synthesis, Crystal Structure, Electronic and Magnetic Properties of $Al_xTi_{1-x}BiO_3$ (0.0 ≤x≤ 0.33) Oxides

Bidhu Bhsuan Das, Ruppa Govinda Rao

Department of Chemistry, Pondicherry University, Pondicherry 605014 (India)

e-mail:das_b_b@yahoo.com

e-mail: govindchem2005@gmail.com

## ABSTRACT

Synthesis of $Al_xTi_{1-x}BiO_3$ (0.0 ≤x≤ 0.33) (S1-S4: x = 0.0, 0.11, 0.22, 0.33) oxides is performed by sol-gel method via nitrate-citrate route. Analysis of the powder X-ray diffraction (XRD) patterns show tetragonal unit cell with lattice parameters: a = 6.6377, 6.6398, 6.6370, 6.6366 Å; c = 6.5445, 6.5391, 6.5259, 6.6583 Å, respectively in S1-S4, with space group P42/mnm and Z=4. Average crystallite sizes determined by Scherrer relation are found to be in the range ~16-36, 18-50, 19-48 and 19-41 nm in S1-S4, respectively. On Rietveld refinement of unit cell structures the agreement factors are lowered to: $R_p$= 98.28, 97.65, 98.85, 94.29 %; $R_{wp}$= 97.11, 96.76, 97.92, 95.73 %; $R_{exp}$= 0.09, 0.09, 0.09, 0.09 % in S1-S4, respectively. Fourier electron density mapping show irregular contours around $Bi^{3+}$, $Ti^{3+}$ and $O^{2-}$ ions due to significant ionic character in Ti-O and Bi-O bonds in the materials. Presence of hysteresis loops in the range -6 kG to +6 kG at 300 K with magnetic susceptibility values in the range 5.926 x $10^{-8}$ - 6.461 x $10^{-8}$ emu/gG in S1-S4 show soft ferromagnetic nature of the oxides. Density functional theory (DFT) calculations using CASTEP (Cambridge Serial Total Energy Package) programme package show energy band gap, $E_g$, ~ 0.01-0.02 eV indicating weak semiconducting nature of the oxides. The valence band (VB) predominantly comprises O 2p, Ti 3d, Al 3p and Bi 6p orbitals, and the conduction band (CB) comprises mostly O 2p, Al 3p and Bi 6p orbitals with extension of band tails narrowing the energy band gap.

## Indexing terms/Keywords

Sol-gel method; powder XRD; crystal structure; DFT calculations; electronic energy band; density of states.

## Academic Discipline And Sub-Disciplines

Chemistry: Physical chemistry

## SUBJECT CLASSIFICATION

Materials chemistry

## TYPE (METHOD/APPROACH)

Experimantal as well as Density functional theory calculations

Council for Innovative Research

Peer Review Research Publishing System

**Journal:** Journal of Advances in Chemistry

Vol. 8, No. 3

editor@cirjac.com

www.jac.cirworld.com, member.cirworld.com

ISSN 2321-807X

## INTRODUCTION

In recent years, nanosized materials, such as nanoparticles, nanowires, nanotubes etc. have received much attention due to their extraordinary electronic, magnetic, optical, and thermal properties **[1-4].** In the domain of nanosized materials, electronic structures of transition metal (TM) containing complex oxides **[5, 6]** have attracted a special attention due to their unusual electronic and magnetic properties with potential applications in next generation magnetic recording media and optical memory devices **[7-9].** Simultaneous presence of strong electron-electron interaction within the TM 3d manifolds and sizeable interaction strength due to thermally excited hopping of electrons between the 3d and oxygen 2p states are primarily responsible for the wide range of properties exhibited by these materials. In this paper, we report on the synthesis, crystal structure, electronic and magnetic properties of $Al_xTi_{1-x}BiO_3$ ($0.0 \leq x \leq 0.33$) non-perovskite oxides **[10]** using direct structure-sensitive techniques such as: powder XRD, differential scanning calorimetry (DSC)/differential thermal analysis (DTA)-thermogravimetric analysis (TGA), scanning electron microscopy (SEM), magnetic measurements, AC electrical conductivity measurements, optical absorption and DFT calculations using CASTEP programme package on the optimized lattice constants and atomic positions.

## EXPERIMENTALS

### Sample Preparation

The samples are prepared by sol-gel method **[11]** via nitrate-citrate route. Stoichiometric amounts of aluminium nitrate, $Al(NO_3)_3$, titanium(III) oxide, $Ti_2O_3$ and bismuth nitrate, $Bi(NO_3)_3{\cdot}5H_2O$, are dissolved in distilled water to prepare 0.1 M solutions each and mixed together. The pH of the resulting solution is adjusted to ~ 2 by adding $HNO_3$. To this solution 30 ml of 1.5 M citric acid solution is added to prepare sol, which is then air dried by stirring continuously at ~ 60 °C for 160 h to form the gel. The resulting gel is decomposed to fine powder at ~ 120 °C which is then heated in air at 450 ºC for 6 h for complete combustion of organic artesia, followed by sintering at 800 °C for 8 h and quenching in air to obtain grey colour fine powder.

### Experimantal Techniques

Powder XRD patterns of the samples are recorded on an X'pert powder X-ray diffractometer (PAN ANALYTICAL make) with scan rate 2°/min in the range 5°-85° in 2θ. Monochromatic Cu Kα radiation (λ ~ 1.5406 Å) is used as the x-ray source with power 40 kV/30 mA. The XRD patterns are analyzed using FullProf Suite (version 3.90) software package **[12]** to determine the unit cell parameters and indexing. Refinement of the unit cell structure is done using Rietveld method **[13].** Fourier electron density mapping of the crystal structure is done using FullProf Suite (version 3.90) software. Microstructures of the materials are examined by a SEM JSM-5410 and Energy dispersive X-ray analysis (EDX) is done by a SUPER DRYER II instrument. DSC/DTA-TGA traces were obtained using a thermal system (DSC/TGA-DTA: TA instrument) (sensitivity of 0.2 µg) in the range 30-1000 °C at heating rate of 10 °C/min in $N_2$ atmosphere. AC electrical conductivity measurements are carried out using a broad band dielectric spectrometer (BDS) (Novocontrol make model concept 80). Magnetic moments of the samples are recorded in the range ±6 kG at 300 K on a LAKESHORE VSM 7404 vibrating sample magnetometer. UV-VIS absorption measurements are performed in range 200-800 nm using a Varian-Model Cary5000 UV-VIS-NIR spectrophotometer. Bulk densities of the samples are determined by liquid displacement method using $CCl_4$ as an immersion liquid (density 1.594 g/cc at 300 K).

### Electronic Energy Band Structure and Density of States (DOS) Calculations

Calculations of electronic energy band structures and DOS are done using a plane-wave DFT with local gradient-corrected exchange-correlation functional **[14]** and performed with a commercial version of the CASTEP programme package **[15-17]**, using Material Studio (MS) software, which uses a plane-wave basis set for the valence electrons and norm-conserving pseudopotential **[18]** for the core states. This program evaluates the total energy of periodically repeating geometries based on DFT and the pseudopotential approximation. In this case only the valence electrons of the elements are represented explicitly in the calculations, and the valence-core interaction being described by nonlocal pseudopotentials.

## RESULTS AND DISCUSSION

### Determination of Unit Cell Parameters

Powder XRD patterns of S1-S4 of $Al_xTi_{1-x}BiO_3$ ($0.0 \leq x \leq 0.33$) oxides are shown in Fig. 1. Using the Fullprof software the phase in the samples is determined and also the indexing of the lattice planes is done. The unit cell in the samples is found to be tetragonal with space group P42/mnm. The unit cell parameters are shown in Table 1 along with the values of experimental densities. Comparison of the experimental density values with those of the calculated ones the value of Z is determined to be 4 in S1-S4. These results show that despite perovskite oxide, $ABO_3$, type compositional formula these materials are non-perovskite oxides **[10]**. Average crystallite sizes in the samples determined by Scherrer relation **[19]** are found to be in the range ~16-36, 18-50, 19-48 and 19-41 nm in S1-S4, respectively which show the formation nanoparticles in the oxides.

ISSN 2321-807X

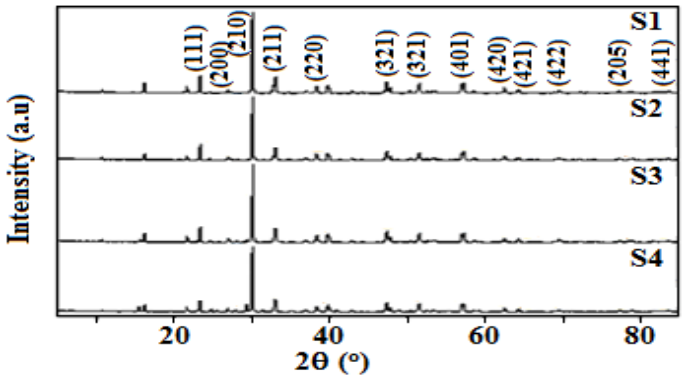


**Fig. 1: Powder XRD patterns and indexed lattice planes of S1-S4 of $Al_xTi_{1-x}BiO_3$(0.0≤x≤ 0.33) oxides.**

**Table 1. Sample compositions, unit cell parameters, observed, $\rho_{obs}$, and calculated, $\rho_{cal}$, densities of S1-S4 of $Al_xTi_{1-x}BiO_3$ (0.00≤x≤ 0.33) oxides.**

| Unit cell parameters | S1 | S2 | S3 | S4 |
|---|---|---|---|---|
| Compositions | $TiBiO_3$ | $Al_{0.11}Ti_{0.89}BiO_3$ | $Al_{0.22}Ti_{0.78}BiO_3$ | $Al_{0.33}Ti_{0.67}BiO_3$ |
| Unit cell type | Tetragonal | Tetragonal | Tetragonal | Tetragonal |
| a*( Å) | 6.6377 | 6.6398 | 6.6370 | 6.6366 |
| c*( Å) | 6.5445 | 6.5391 | 6.5259 | 6.6583 |
| Unit cell volume ($Å^3$) | 288.345 | 288.289 | 287.464 | 293.261 |
| Space group | P42/mnm | P42/mnm | P42/mnm | P42/mnm |
| Z | 4 | 4 | 4 | 4 |
| $\rho_{cal}$ (g/cc) | 7.023 | 6.903 | 6.801 | 6.547 |
| $\rho_{obs}$ (g/cc) | 6.748 | 6.659 | 6.854 | 6.407 |

*after refinement

## Microstructures, EDX and Thermal Analysis

SEM micrographs of selected samples S1 and S4 are shown in Fig. 2 (a, b), which show irregular globular agglomerated particles in S1(x=0.0) through S4 (x=0.33). Various localized regions of the samples also show similar microstructures with respect to the particle sizes and shapes. Fig. 2 (c) shows the EDX profile of S4. Presence of the constituent elements Al, Ti, Bi and O only in the profile show the purity of the samples. Fig. 3 shows the DSC/DTA-TGA traces of S1 and S4 in the range 50-1000 °C. Abrupt weight loss in the TGA traces of S1 in the range 105 to 420 °C with no characteristic peak in the DSC/DTA traces is attributed to the removal of physically and chemically adsorbed water in the sample. Further at higher temperatures upto 900 $^oC$ absence of any characteristic event in the DSC/DTA-TGA traces show the thermal stability of the samples upto 900 $^oC$. Furthermore, weight loss in the samples ~ 900 °C could be due to the decomposition of the samples.

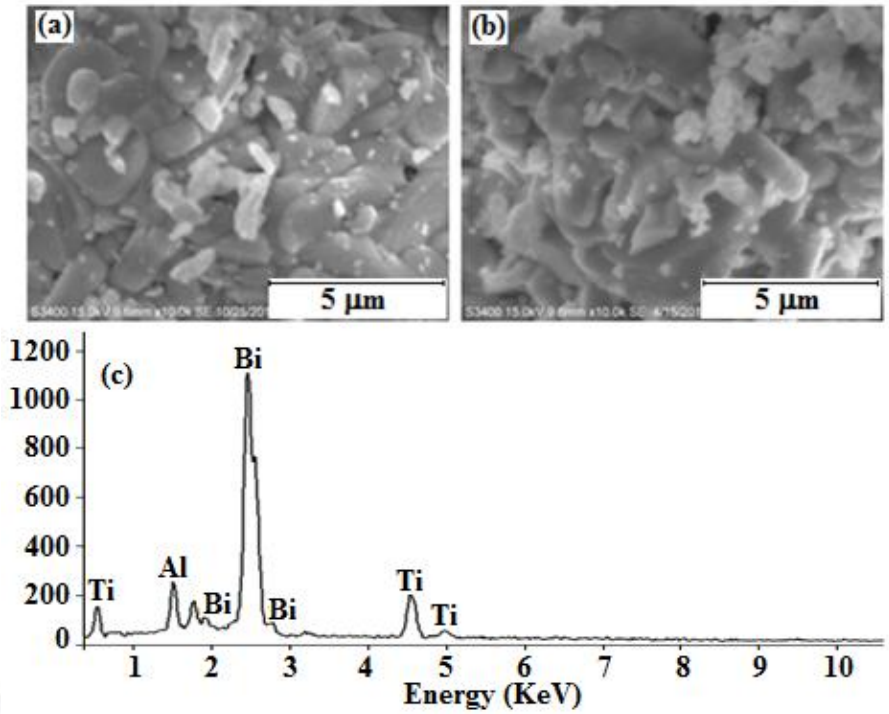


**Fig. 2. SEM micrographs of selected samples (a) S1 (x=0.0), (b) S4 (x=0.33) at same magnification and (c) EDX profile of $Al_{0.33}Ti_{0.67}BiO_3$ (S4).**

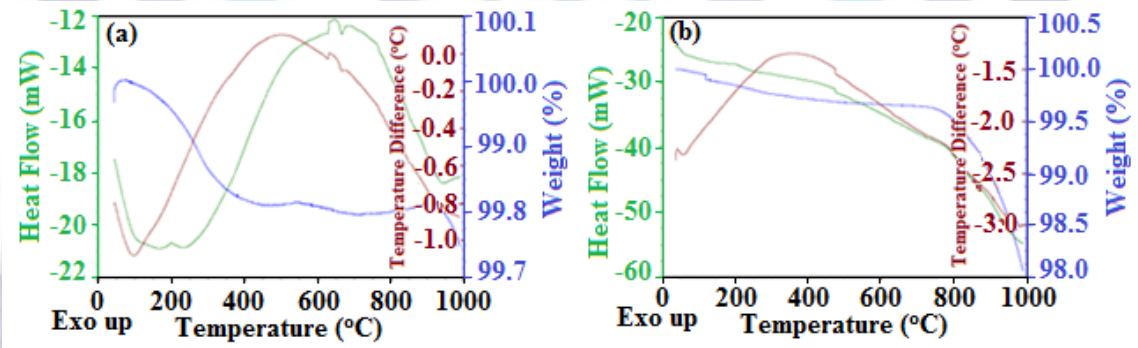


**Fig. 3: DSC/DTA-TGA traces of (a) $TiBiO_3$ (S1) and (b) $Al_{0.33}Ti_{0.67}BiO_3$ (S4).**

## Crystal Structure Refinement and Fourier Electron Density Mapping

Unit cell structures of S1-S4 are developed on space group P42/mnm with $Ti_1^{3+}(Al_1^{3+})$ ions in 2(a), $Ti_2^{3+}(Al_2^{3+})$ ions in 4(c), $Bi^{3+}$ ions in 4(f) and $O^{2-}$ ions in 2(b), 4(d) and 8(j) Wycoff sites. Site occupancies of the ions are set according to the stoichiometry. On Rietveld refinement **[13]**, the various agreement factors are lowered to: $R_p$ (%) = 98.28, 97.65, 98.85, 94.25 %; $R_{wp}$ (%) = 97.11, 96.76, 97.92, 95.73; $R_{exp}$ (%) = 0.09, 0.09, 0.09, 0.09 in S1-S4, respectively, and the lattice parameters are shown in Table 1. 3-dimensional view of the unit cell structure of S4 (x=0.33) is shown in Fig. 4 (a) along with the projection onto (001) plane (Fig. 4 (b)). The above views in all the samples S1-S4 are similar. The crystal coordinates and the cartesian coordinates before and after refinement, the bond lengths and the bond angles in the unit cell structures are shown in Tables 2, 3 and 4, respectively. The various bond lengths and bond angles in the asymmetric units of S1-S4 show only marginal variation due to variations in compositions. 3-dimensional Fourier electron density mapping from <001> plane of S4 (x=0.33) and the 2-dimensional electron density contour on (001) plane are shown in Fig. 4 (c, d). Irregular electron density contours around the $Ti^{3+}$, $Bi^{3+}$, and $O^{2-}$ ions show the significant ionic characters in the Ti-O and Bi-O bonds in the materials.

ISSN 2321-807X

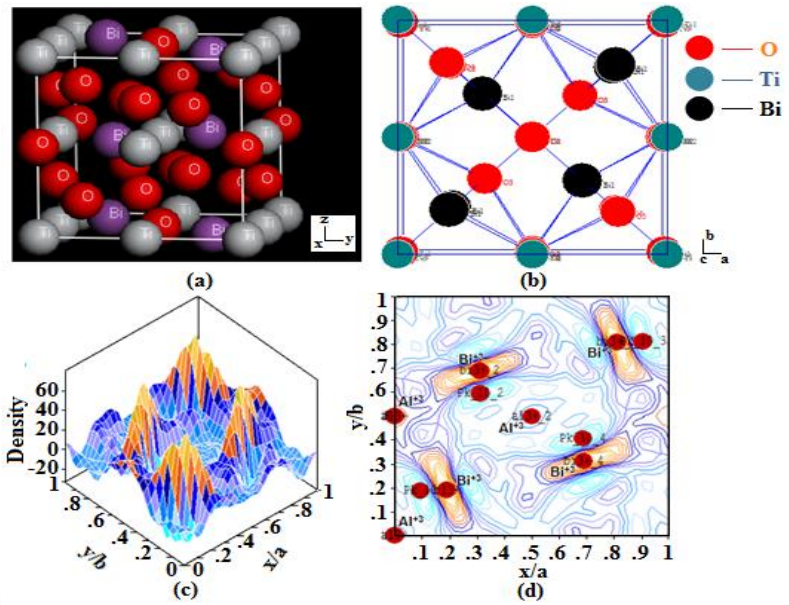


**Fig. 4: (a) 3-dimensional view, (b) 2-dimensional view on (001) plane, (c) 3-dimensional electron density from <001> plane, and (d) 2-dimensional electron density contour on (001) plane of $Al_{1.32}Ti_{2.68}Bi_4O_{12}$ (S4: x=0.33) unit cell structure.**

**Table 2. Generated crystal coordinates (XYZ) and cartesian coordinates (xyz) before and after refinement of the atomic positions in the asymmetric units in S1-S4 of $Al_xTi_{1-x}BiO_3$ (0.0≤x≤0.33) oxides.**

| Sample | Atoms | Crystal coordinates | | | Cartesian coordinates before refinement | | | Cartesian coordinates after refinement | | |
|---|---|---|---|---|---|---|---|---|---|---|
| | | X | Y | Z | x | y | z | x | y | z |
| **S1** | | | | | | | | | | |
| **1** | Ti1 | 0.0000 | 0.0000 | 0.0000 | -3.3167 | -3.2743 | -3.2743 | -3.3189 | -3.3189 | -3.2722 |
| **2** | Ti2 | 0.0000 | 0.5000 | 0.0000 | -3.3167 | 0.0000 | -3.2743 | -3.3189 | 0.0000 | -3.2722 |
| **3** | Bi1 | 0.1900 | 0.1900 | 0.0000 | -2.0564 | -2.0564 | -3.2743 | -2.0577 | -2.0577 | -3.2722 |
| **4** | O1 | 0.0000 | 0.0000 | 0.5000 | -3.3167 | -3.3166 | 0.0000 | -3.3189 | -3.3189 | 0.0000 |
| **5** | O2 | 0.0000 | 0.5000 | 0.2500 | -3.3167 | 0.0000 | -1.6372 | -1.1952 | -1.1948 | -1.1780 |
| **6** | O3 | 0.3200 | 0.3200 | 0.3200 | -1.1940 | -1.1940 | -1.1787 | -1.1948 | -1.1948 | -1.1780 |
| **S2** | | | | | | | | | | |
| **1** | Ti1 | 0.0000 | 0.0000 | 0.0000 | -3.3189 | -3.3189 | -3.2722 | -3.3200 | -3.3199 | -3.2696 |
| **2** | Ti2 | 0.0000 | 0.5000 | 0.0000 | -3.3189 | 0.0000 | -3.2722 | -3.3199 | 0.0000 | -3.2696 |
| **3** | Bi1 | 0.1900 | 0.1900 | 0.0000 | -2.0577 | -2.0577 | -3.2722 | -2.0584 | -2.0584 | -3.2696 |
| **4** | O1 | 0.0000 | 0.0000 | 0.5000 | -3.3189 | -3.3189 | 0.0000 | -3.3199 | -3.3199 | 0.0000 |
| **5** | O2 | 0.0000 | 0.5000 | 0.2500 | -3.3189 | 0.0000 | -1.6361 | -3.3199 | 0.0000 | -1.6348 |
| **6** | O3 | 0.3200 | 0.3200 | 0.3200 | -1.1948 | -1.1948 | -1.1787 | -1.1952 | -1.1952 | -1.1770 |
| **S3** | | | | | | | | | | |
| **1** | Ti1 | 0.0000 | 0.0000 | 0.0000 | -3.3165 | -3.3164 | -3.2641 | -3.3186 | -3.3185 | -3.2629 |
| **2** | Ti2 | 0.0000 | 0.5000 | 0.0000 | -3.3164 | 0.0000 | -3.2641 | -3.3185 | 0.0000 | -3.2629 |
| **3** | Bi1 | 0.1900 | 0.1900 | 0.0000 | -2.0562 | -2.0562 | -3.2641 | -2.0575 | -2.0575 | -3.2629 |

ISSN 2321-807X

| | | | | | | | | | | |
|---|---|---|---|---|---|---|---|---|---|---|
| **4** | O1 | 0.0000 | 0.0000 | 0.5000 | -3.3164 | -3.3164 | 0.0000 | -3.3185 | -3.3185 | 0.0000 |
| **5** | O2 | 0.0000 | 0.5000 | 0.2500 | -3.3164 | 0.0000 | -1.6321 | -3.3185 | 0.0000 | -1.6315 |
| **6** | O3 | 0.3200 | 0.3200 | 0.3200 | -1.1939 | -1.1939 | -1.1751 | -1.1947 | -1.1947 | -1.1947 |
| **S4** | | | | | | | | | | |
| **1** | Ti1 | 0.0000 | 0.0000 | 0.0000 | -3.3134 | -3.3134 | -3.3373 | -3.3184 | -3.3183 | -3.3291 |
| **2** | Ti2 | 0.0000 | 0.5000 | 0.0000 | -3.3134 | 0.0000 | -3.3373 | -3.3183 | 0.0000 | -3.3291 |
| **3** | Bi1 | 0.1900 | 0.1900 | 0.0000 | -2.0543 | -2.0543 | -3.3373 | -2.0574 | -2.0574 | -3.3291 |
| **4** | O1 | 0.0000 | 0.0000 | 0.5000 | -3.3164 | -3.3373 | 0.0000 | -3.3183 | -3.3183 | 0.0000 |
| **5** | O2 | 0.0000 | 0.5000 | 0.2500 | -3.3134 | 0.0000 | -1.6687 | -3.3183 | 0.0000 | -1.6646 |
| **6** | O3 | 0.3200 | 0.3200 | 0.3200 | -1.1928 | -1.1928 | -1.2014 | -1.1946 | -1.1946 | -1.1985 |

**Table 3. Bond lengths (Å) in asymmetric units of S1-S4 of $Al_xTi_{1-x}BiO_3$(0.0≤x≤0.33) oxides**

| Sl. No. | Atoms | S1 | S2 | S3 | S4 |
|---|---|---|---|---|---|
| **1** | Ti2-O2 | 1.6361(1) | 1.6348(1) | 1.6315(1) | 1.6646(1) |
| **2** | Bi1-O3 | 2.4239(1) | 2.4226(1) | 2.4187(1) | 2.4553(1) |

**Table 4. Bond angles in degrees in asymmetric units of S1-S4 of $Al_xCe_{1-x}BiO_3$(0.0 ≤x≤ 0.33) oxides.**

| Sl. No. | Atoms | S1 | S2 | S3 | S4 |
|---|---|---|---|---|---|
| **1** | O2-Ti2-O3 | 49.3261(1 | 49.3584(1) | 49.4037(1) | 48.8325(1) |
| **2** | Ti2-O3-Bi1 | 55.8654(1) | 55.8958(1) | 55.9383(1) | 47.7709(1) |
| **3** | O1-Bi1-O2 | 66.4059(1) | 66.4452(1) | 66.5002(1) | 65.8052(1) |
| **4** | O1-Bi1-O3 | 58.8226(1) | 58.8785(1) | 58.9570(1) | 57.9736(1) |
| **5** | O2-Bi1-O3 | 54.4025(1) | 54.4308(1) | 54.4704(1) | 53.9692(1) |

## Band Structure and Density of State (DOS)

Electronic energy band structures due to chemical bonding, valence electrons distribution in atoms and electron localization function could provide physical insight into the structural and other related properties. Fig. 5 (a, b) shows the electronic energy band structures and the DOS of S1, while Fig. 5 (c, d) shows the energy band structures and the DOS of S4. The Fermi level is set at 0 eV. A smearing of 0.5 eV is used to generate the DOS plots. It can be noted that the samples do not have clear band gap. The band tails cross the Fermi energy levels. This shows the very weak semiconducting nature of the materials. Fig. 6 shows the calculated total DOS and partial DOS of elements O, Ti, Al, and Bi in $Al_{0.33}Ti_{0.67}BiO_3$(S4: x=0.33). The plane-wave basis set is generated with valence configurations of Ti-$3s^2 3p^6 3d^2 4s^2$, O-$2s^2 2p^4$, Al-$3s^2 3p^1$ and Bi-$5s^2 5p^6 5d^{10} 6s^2 6p^3$. The high DOS of valence band (VB) located at -7.60 to 0.0 eV is due to the Al 3s, 3p; Ti 4s, 3d; Bi 6s, 6p and O 2s, 2p orbitals. The DOS of conduction band (CB) located at ~ 0.0 to 2.82 eV is due to Ti 3d; Al 3p; Bi 6s, 6p and O 2p orbitals. The band structure clearly shows that there is a very high DOS located at about -7.60 to 1.55 eV due to the overlap of CB and VB at band tails, predominantly due to O 2p; Al 3p and Bi 6s and 6p orbitals **[20, 21]** with significant contribution from Ti 3d orbitals in the range -7.1 to 1.13 eV. Contribution from Bi 6s, 6p states in the VB suggests hybridization in accordance with the covalent bond formation in Bi–O **[22]** bond. The Ti 3d-states are slightly above the Fermi level. The DOS peak, 5 states (electrons/eV), located at 2.25 eV above the Fermi level mainly is mainly from the Ti 3d orbitals with slight contribution Bi 6p orbitals. As the bands cross over the Fermi level without any clear band gap, the samples are possibly very weak semiconducting in nature as mentioned earlier. The core bands in the range -19.45 to -9.45 eV are formed from the valence orbitals of O, Bi and Al.

ISSN 2321-807X

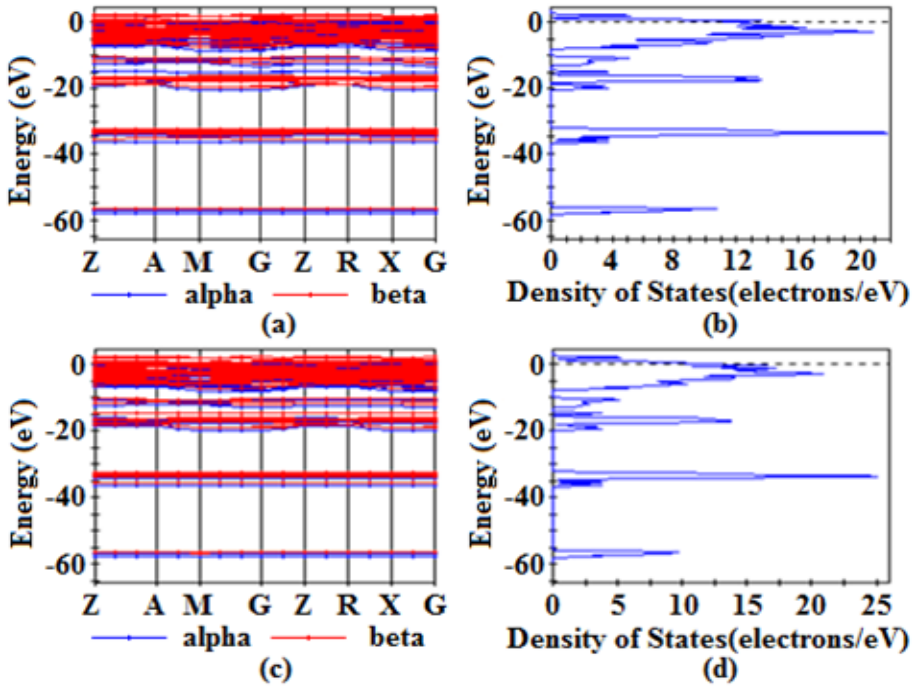


**Fig. 5. (a) Band structure and (b) DOS of $TiBiO_3$ (S1); and (c) band structure and (d) density of states of $Al_{0.33}Ti_{0.67}BiO_3$(S4).**

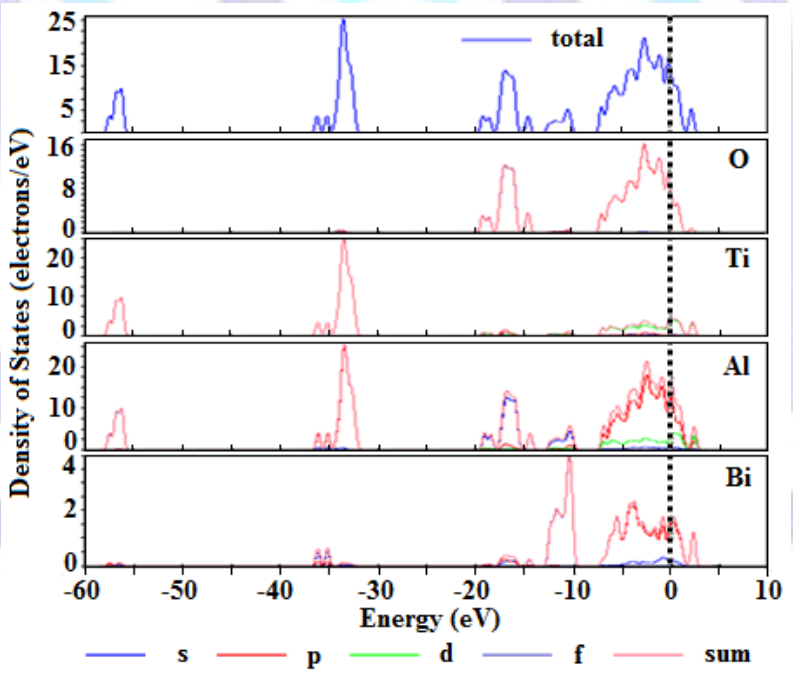


**Fig. 6. Calculated total and partial DOS of the elements, O, Ti, Al and Bi in $Al_{0.33}Ti_{0.67}BiO_3$ (S4: x= 0.33).**

## AC and DC Electrical Conductivity

The complex AC conductivity **[23, 24]**, σ*, is given by,

$$\sigma^*(f) = \sigma'(f) + \sigma''(f) \qquad (1)$$

where σ′ is the real part and σ″ is the imaginary part. The real part σ′ is called the AC conductivity. Fig. 7 (a-d) shows the plots of σ′(S/cm) versus log f (Hz) of S1-S4 at different temperatures. Each of the plots was extrapolated to zero frequency to obtain the DC electrical conductivity, $\sigma_{dc}$, for the sample at that temperature. From the DC electrical conductivity data, log $\sigma_{dc}$ versus $10^3/T$ ($K^{-1}$) plots (Fig. 8) are obtained for all the samples using the Arrhenius equation.

ISSN 2321-807X

$$\sigma_{dc} = \sigma_o \exp(-E_a/kT) \quad (2)$$

where $E_a$ is the activation energy, k is the Boltzmann constant and T is the absolute temperature. The plots show nearly straight line behaviour and the slopes are obtained from the linear fit of the plots. From the slopes the values of the activation energy, $E_a$, of the samples are found to be 0.225, 0.318, 0.357 and 0.446 in S1-S4, respectively. This result shows that the samples are weak semiconductors, and the semiconductivity increases from S1 ($TiBiO_3$) to S4 ($Al_{0.33}Ti_{0.67}BiO_3$) with the progressive substitution of $Al^{3+}(2p^6)$ ions in $Ti^{3+}(3d^1)$ sites. The result further shows that the semiconductivity arises from partial delocalization of the single $3d^1$ electron at $Ti^{3+}$ sites which are linked through the bridging $O^{2-}$ ions to the $Bi^{3+}$ sites (Ti-O-Bi) in the crystalline lattice. Thus incorporation of $Al^{3+}$ ions result in the formation of Al-O-Bi bridge containing only the localized electrons in the stable ions in the crystalline solid matrix thereby the delocalization of number of hopping electrons is reduced and consequently semiconductivity is enhenced. It may be mentioned that the calculated values of the energy band gap, $E_g$, by CASTEP from the unit cell structures are found to be ~ 0.02 eV in S1-S4 which are much lower than the values obtained by observed electrical conductivity data as above. This inconsistency is due to the drawback of the DFT calculations in such complex oxide systems.

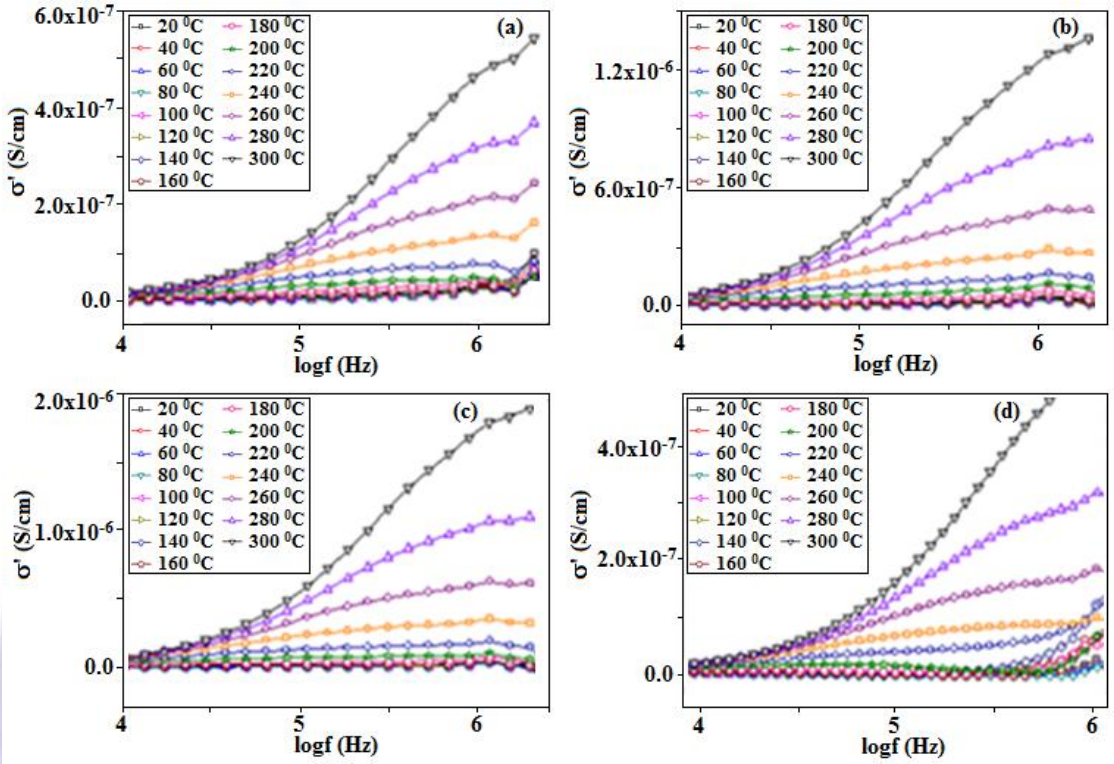


**Fig. 7: Frequency dependent AC conductivity at different temperatures for (a) S1(x=0.00), (b) S2(x=0.11), (c) S3(x=0.22), (d) S4(x=0.33) of $Al_xTi_{1-x}BiO_3$ (0.0 ≤x≤ 0.33) oxides.**

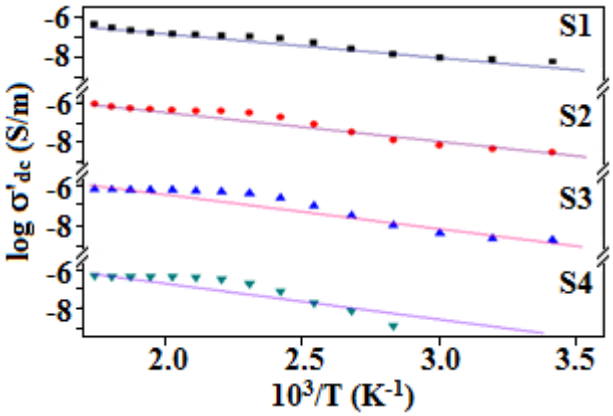


**Fig. 8: Temperature dependent DC electrical conductivity plots of S1-S4 of $Al_xTi_{1-x}BiO_3$ (0.0 ≤x≤ 0.33) oxides.**

ISSN 2321-807X

## Dielectric Properties

The complex dielectric function, ε*, is given by,

$$\varepsilon^* = \varepsilon' + i\varepsilon'' \qquad (3)$$

where the real part ε′ is called the dielectric constant, and the imaginary part, ε″, is called the dielectric loss factor due to conduction process. Fig. 9 (a-d) shows the plots of real part, ε′, and imaginary part, ε″, of dielectric loss of S1 (x=0.0) and S4 (x=0.33) at different temperatures from 20-300 $^{o}$C versus AC frequencies. At higher temperatures near 300 $^{o}$C the ε′ decreases rapidly with increasing AC frequency in S1 and S4, while at lower temperatures near room temperature, ε′ decreases marginally with increasing frequencies. Furthermore, ε′ increases with increasing temperatures from 20 $^{o}$C to 300 $^{o}$C at a fixed AC frequency with significant increase at lower frequencies to marginal increase at higher frequencies (~ $10^7$ Hz). This result shows that thermally activated hopping **[23]** of $Ti^{3+}(3d^1)$ electron is the prime factor for AC conductivity in these systems. Also at higher temperatures upto 300 $^{o}$C relatively more ordered orientation of the electric dipoles enhances the increased values of ε′. It is also important to mention that these rigid non-viscous systems do not exhibit ideal Debye-type pattern of the ε′ versus frequency (Hz) plots (Fig. 9 (a, c)) which indicates that electronic conductivity in these systems is significant as compared with the ionic conductivity. However, as compared with S1(x=0.0) ($TiBiO_3$) the sample S4(x=0.33) ($Al_{0.33}Ti_{0.67}BiO_3$) shows slight indication of Debye-type peak formation at mid-frequency ranges. This could be due to some contribution in ionic conductivity from the mobile $Al^{3+}$ ions in S4 due to smaller ionic radius.

Fig. 9 (b, d) shows that the dielectric loss factor, ε″, increases with the increasing temperatures at a fixed frequency, f (Hz), and decreases rapidly for high temperature cases with increasing frequencies as compared with the decrease at lower temperatures with less prominent Debye-type peak in the upper mid range frequencies in S1 and S4. This result could also be attributed to the enhanced ordering of the electric dipoles at higher temperatures as discussed in the case of dielectric permittivity, ε′. The ε″ versus f (Hz) plots normally show a peak in the mid frequency range which is called the relaxation peak. In Fig. 9 (b, d) a very less prominent such peak is observed at lower temperatures. However, the peak shifts towards higher frequencies with increasing temperatures. This result shows that very less significant ionic conductivity takes place in these materials within the temperature range studied in contrast to other systems reported by earlier workers **[23].**

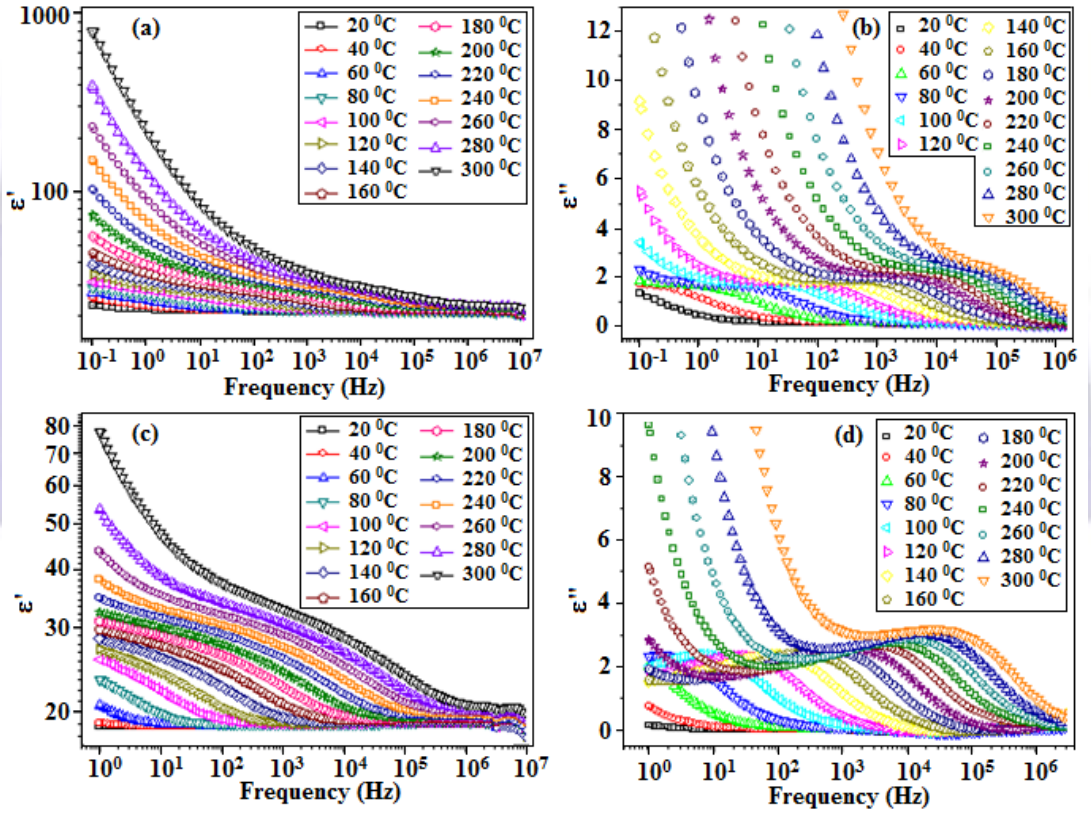


**Fig. 9. Plots of (a) real part dielectric constant, ε′, at different temperatures for S1(x = 0.00), (b) dielectric loss, ε″, at different temperatures for S1(x = 0.00), (c) real part dielectric constant, ε′, at different temperatures for S4(x = 0.33), (d) dielectric loss, ε″, at different temperatures for S4(x = 0.33), versus AC frequencies.**

## Magnetic Properties

Fig. 10 shows the field dependence of magnetization (M–H) curves of S1-S4 of $Al_xTi_{1-x}BiO_3$ (0.0 ≤x≤ 0.33) oxides measured at 300 K. Formation of hysteresis loops indicate the soft ferromagnetic nature in S1-S4 at 300 K. The M–H loops are analysed in the low-field region (±6.0 kG) and the values of saturation magnetization (Ms), coercivity (Hc), and

remanent magnetization (Mr) and the calculated magnetic susceptibility ($\chi$) of S1-S4 at 300 K are shown in Table 5. The table shows that the above magnetic properties in the samples show only marginal variation which indicates the weak ferromagnetic nature of the materials.

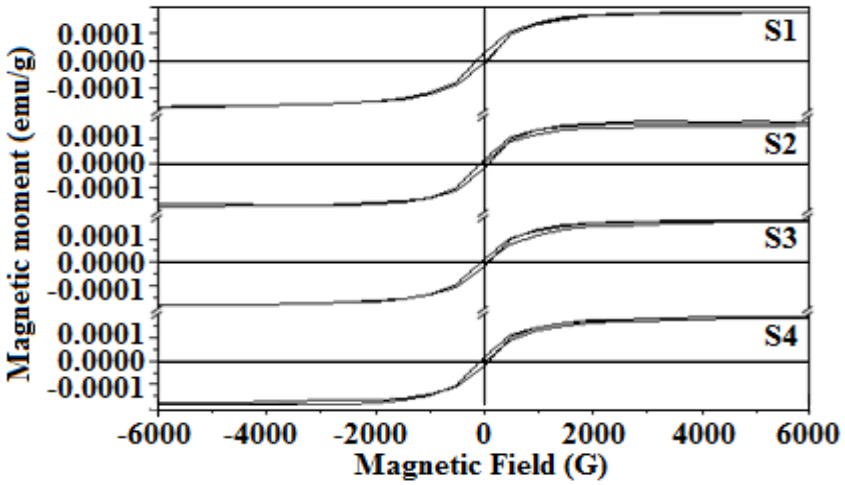


**Fig. 10. Magnetic moment versus Magnetic field plots of S1-S4 of $Al_xTi_{1-x}BiO_3$ (0.0 ≤x≤ 0.33) oxides measured at 300 K.**

**Table 5. Values of magnetization (Ms), coercivity (Hc), retentivity (Mr) and magnetic susceptibility, χ, values of S1–S4 of $Al_xTi_{1-x}BiO_3$ (0.0 ≤x≤ 0.33) oxides at 300 K.**

| Magnetic properties | S1 | S2 | S3 | S4 |
|---|---|---|---|---|
| Saturation magnetization (Ms x$10^{-6}$ (emu/g) | 176.090 | 178.250 | 183.140 | 191.500 |
| Coercivity (Hc) (G) | 86.172 | 86.715 | 86.256 | 76.536 |
| Retentivity (Mr) x $10^{-6}$ (emu/g) | 18.202 | 21.075 | 16.673 | 18.556 |
| Magnetic susceptibility ($\chi$) x $10^{-8}$ (emu/gG) | 5.990 | 5.926 | 6.135 | 6.461 |

## Optical Absorption Spectroscopy

Room temperature optical absorbance spectra of S1-S4 are shown in Fig. 11(a). The samples show overlapped absorption bands ~ 200-350 nm. The peak ~220 nm is due to the $O^{2-} \rightarrow Ti^{3+}$ charge transfer band. The broad absorption band ~ 290 nm is commonly assigned to the $Bi^{+3}(5d^{10}6s^2)$ $^1S_0 \rightarrow {}^3P_1$ electronic transition **[25].** The broad band ~ 320 nm is attributed to the $Ti^{3+}(3d^1)$ ions **[26]**. Fig. 11 (b) shows the plots of $(\alpha h\nu)^2$ versus hν of S1-S4 where α is the absorption coefficient. The energy band gap, $E_g$, in the materials are obtained by extrapolating the linear part of the plots to the photon energy axis (Fig. 11 (b)). The obtained $E_g$ values are: 2.92, 2.85, 2.84, and 2.91 eV in S1-S4, respectively. However, the $E_g$ values calculated from the unit cell structure by DFT are of the order of ~0.02 eV in the samples. This discrepancy/underestimation is due to the known limitations of the DFT calculations which involves exchange correlation functions.

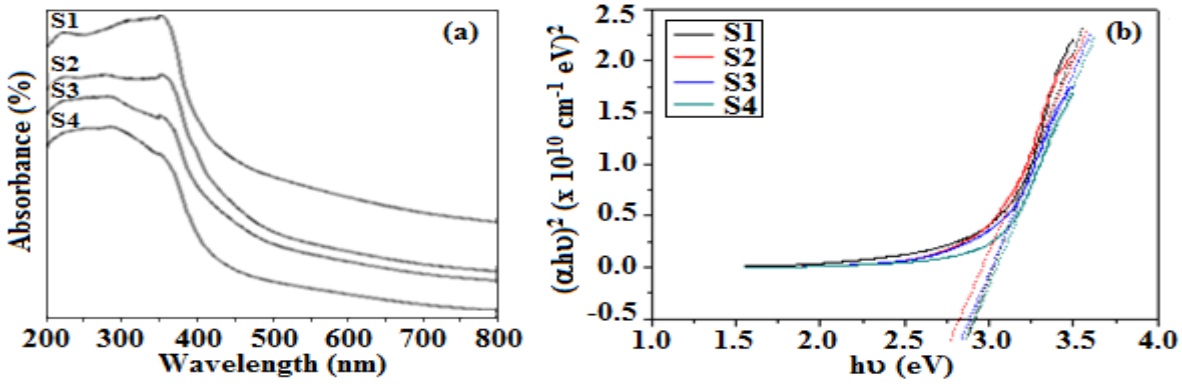


**Fig. 11: (a) Optical absorption spectra (b) band gap energy calculation by plotting $(\alpha h\nu)^2$ versus hν of S1-S4 of $Al_xTi_{1-x}BiO_3$ (0.0 ≤x≤ 0.33) oxides.**

## Conclusion

Non-perovskite oxides in the series $Al_xTi_{1-x}BiO_3$($0.0 \leq x \leq 0.33$) are prepared via sol-gel method. Powder XRD results show tetragonal phase with space group P42/mnm and Z=4. Average crystallite sizes in the range ~16-36, 18-50, 19-48 and 19-41 nm in S1-S4 show the formation of nanosize particles. DSC/DTA-TGA results show no phase transitions in the range 450-900 ºC. Rietveld refinement of the unit cell structures developed in space group P42/mnm with Z = 4 show appreciable lowering of agreement factors $R_p$, $R_{wp}$ and $R_{exp}$ for the samples. Plane-wave DFT calculations on unit cell structures for band structures and DOS show the $E_g$ ~ 0.02 eV in S1-S4 indicating the weak semiconducting nature of the samples. Fourier mapping of 2-dimensional electron density irregular contours on (001) plane show the significant ionic nature of the Bi-O and Ti-O bonds. Magnetic studies show the formation of hysteresis loops with relatively low values of the related parameters indicates the soft ferromagnetic nature of the materials at 300 K. The broad optical absorption band ~290 nm is due to $Bi^{+3}\ ^1S_0 \rightarrow {}^3P_1$ transition.

## ACKNOWLEDGMENTS

The authors thank Dr. M. M. Balakrishnarajan, for help with the Materials Studio software.

## REFERENCES

[1] Hua, Y., Liu, Y., Jiang, G., Du, J., and Chen, J. J. 2013. Geometric transition and electronic properties of titanium-doped aluminum clusters: $Al_nTi$ (n = 2−24). Phys. Chem. A 117 (Mar. 2013), 2590-2597.

[2] Ali, M. S., Islam, A. K. M. A., Hossain, M. M., and Parvin, F. 2012. Phase stability, elastic, electronic, thermal and optical properties of $Ti_3Al_{1-x}Si_xC_2$ ($0 \leq x \leq 1$): First principle study. Physica B 407 (Nov. 2012), 4221-4228.

[3] Shi, C., Liu, X., Hao, Y., and Hu, Z. 2011. Structural, magnetic and dielectric properties of $Bi_{1-y}Sr_yFe_{(1-y)(1-x)}Sc_{(1-y)x}Ti_yO_3$ (x = 0-0.2, y = 0.1-0.3) ceramics. Mater. Res. Bull. 46 (Mar. 2011), 378-383.

[4] Mao, Y., Park, T. J., and Wong, S.S. 2005. Synthesis of classes of ternary metal oxide nanostructures. Chem. Commun. 46 (Nov. 2005), 5721–5735.

[5] Gulden, C., and Suleyman, C. 2013. First-principles study of electronic structure and optical properties of $Sr(Ti,Zr)O_3$. Cent. Eur. J. Phys. 11(3) (Mar. 2013), 387–393.

[6] Nohara, Y., Yamamoto, S., and Fujiwara, T. 2009. Electronic structure of perovskite-type transition metal oxides $LaMO_3$ (M=Ti~Cu) by U+GW approximation. Phys. Rev. B 79 (May 2009), 195110−195114.

[7] Ohkoshi, S., Tsunobuchi, Y., Matsuda, T., Hashimoto, K., Namai, A., Hakoe, F., and Tokoro, H. 2010. Synthesis of a metal oxide with a room temperature photoreversible phase transition. Nat. Chem. 2 (May 2010), 539–545.

[8] Sevincli, H., Topsakal, M., Durgun, E., and Ciraci, S. 2008. Electronic and magnetic properties of 3d transition-metal atom adsorbed grapheme and graphene nanoribbons. Phys. Rev. B 77 (May 2008), 195434–195437.

[9] Osaka, T., and Sayama, J. 2007. A challenge of new materials for next generation's magnetic recording. Electrochim. Acta. 52 (Feb. 2007), 2884–2890.

[10] Tanaka, M., Shishido, T., Horiuchi, H., Toyota, N., Shindo, D., and Fukuda, T. J. 1993. Structure studies of of $CeAl0_3$. Alloys Compd. 192 (Feb. 1993), 87–89.

[11] Hench, L. L., and West, J. K. 1990. The sol-gel process. Chem. Rev. 90 (Jan. 1990), 33–72.

[12] Roisnel, T., and Carvajal, J. R. 2001. WinPLOTR: A Windows Tool for Powder Diffraction Pattern Analysis Mater. Sci. Forum. 378-381 (Jan. 2001), 118–123.

[13] McCusker, L. B., Von Dreele, R. B., Cox, D. E., Louer, D., and Scardi, P. J. 1999. Rietveld refinement guidelines. J. Appl. Cryst. 32 (Feb. 1999), 36-50.

[14] Perdew, J. P., Burke, K., and Ernzerhof, M. 1996. Generalized Gradient Approximation Made Simple. Phys. Rev. Lett.77 (Oct. 1996), 3865–3868.

[15] Clark, S. J., Segall, M. D., Pickard, C. J., Hasnip, P. J, Probert, M. I. J., Refson, K., and Payne, M. C. 2005. First principles methods using CASTEP. Z. Kristallogr. 220(5-6) (Sep. 2009), 567- 570.

[16] Segall, M. D., Lindan, P. L. D., Probert, M. I. J., Pickard, C. J., Hasnip, P. J., Clark, S. J., and Payne, M. C. 2002. First-principles simulation: ideas, illustrations and the CASTEP code. J. Phys.: Cond. Matt.14 (Mar. 2002), 2717- 274.

[17] Payne, M. C., Teter, M. P., Allan, D. C., Arias, T. A., and Joannopoulos, J. D. 1992. Iterative minimization techniques for ab initio total energy calculations: molecular dynamics and conjugate gradients. Rev. Mod. Phys. 64 (Oct. 1992), 1045-1097.

[18] Hamman, D. R., Schlüter, M., and Chiang, C. 1979. Norm-Conserving Pseudopotentials. Phys. Rev. Letts. 43 (Nov. 1979), 1494-1497.

[19] Klug, H. P., and Alexander, L. E., 1997. X-ray Diffraction procedures for polycrystalline and amorphous Materials, 2nd ed., John Wiley & Sons. Ltd, New York, p.966.

[20] Li, D., Zheng, J., and Zou, Z. J. 2006. Band structure and photocatalytic properties of perovskite-type compound $Ca_2NiWO_6$ for water splitting. Phys. Chem. Solids 67 (Jan. 2006), 801-806.

[21] Wang, C. B., Nisar, J., Pathak, B., Kang, W. T., and Ahuja, R. 2012. Band gap engineering in $BiNbO_4$ for visible-light photocatalysis. Appl. Phys. Lett. 100 (Apr. 2012), 182102–182105.

[22] Farias, S. A. S., and Martins, J. B. L. 2012. Bonding and electronic structure of sillenites. J. Chem. Phys. Lett. 533(Apr. 2012), 78–81.

[23] Jayswal, M. S., Kanchana, D. K., Sharma, P., and Gondaliya, N. 2013. Relaxation process in $PbI_2$–$Ag_2O$–$V_2O_5$–$B_2O_3$ system: Dielectric, AC conductivity and modulus studies Mater. Sci. Eng. B 178 (Jun. 2013), 775– 784.

[24] Jayswal, M. S., Kanchana, D. K., Sharma, P., and Pant, M. 2011. The effect of $PbI_2$ on electrical conduction in $Ag_2O$-$V_2O_5$-$B_2O_3$ superionic glass system. Solid State Ionics 186(1) (Mar. 2011), 7–13.

[25] Lacklison, D. E., Scott, G.B., and Page, J.L.1974. Absorption Spectra of $Bi^{3+}$ and $Fe^{3+}$ in $Y_3Ga_5O_{12}$. Solid. State. Commun. 14(9) (May 1974), 861–863.

[26] Wu, J., Yue, G., Xiao, Y., Lin, J., Huang, M., Lan, Z., Tang, Q., Huang, Y., Fan, L., Yin, S., and Sato, T. 2013. An ultraviolet responsive hybrid solar cell based on titania/poly(3-hexylthiophene). Sci. Rep. 3 (Feb. 2013), 1283–1288.

## Author' biography with Photo

Prof. Bidhu Bhusan Das did his 5-Yr. M. Sc. in Chemistry in 1982 and Ph. D. in electron paramagnetic resonance (EPR) and materials chemistry from Indian Institute of Technology Kanpur in 1987. He was a Postdoctoral Fellow (under 35 yrs.) of the Commission of the European Communities in ISMRA Caen during 1992-93 and did his research work in Materials chemistry and powder X-ray crystallography. Prof. Bidhu Bhusan Das served as faculty member in Chemistry in Pondicherry University, Puducherry, University of Hyderabad, Hyderabad and University of Delhi, Delhi in India since 1987. At present, Prof. Bidhu Bhusan Das is a professor in Chemistry in Pondicherry University, Puducherry, India. Prof. Bidhu Bhusan Das has research publications in national and international journals. His research specialization is structure-property relations in electronic and magnetic materials and EPR spectroscopy.

Ruppa Govinda Rao obtained his M. Sc. degree in Chemical Sciences from the Department of Chemistry, Pondicherry University, Puducherry, India in 2007. Presently, he is perusing his Ph.D. research under the guidance of Prof. Bidhu Bhusan Das, in Functional Materials Chemistry, Department of Chemistry, Pondicherry University, Puducherry, India. His research interests are sol-gel synthesis, crystal structure, magnetic, electronic and optical properties of nano oxides.